Ind. J. Pharm. Edu. Res., 2024; 58(3s):s944-s962.
https://www.ijper.org

Original Article

Biosynthesis of Silver Nanoparticles from *Canavalia rosea* and its Antiproliferative Effect on MCF-7 Cancer Cell Line

Vasanthi R[1,*], Balamurugan V[1], Hesham S. Almoallim[2], Sulaiman Ali Alharbi[3]

[1] PG & Research, Department of Biotechnology, Sri Vinayaga College of Arts and Science (Affiliated to Thiruvalluvar University, Serkkadu, Vellore), Ulundurpet, Tamil Nadu, INDIA.
[2]Department of Oral and Maxillofacial Surgery, College of Dentistry, King Saud University, Riyadh, SAUDI ARABIA.
[3]Department of Botany and Microbiology, College of Science, King Saud University, Riyadh, SAUDI ARABIA.

ABSTRACT

Aim: The generation of silver nanoparticles via a green synthesis approach with leaf and stem extracts of *Canavalia rosea* is our prime objective. **Materials and Methods:** The fabricated Nanoparticles (AgNPs) are interpreted by Gas Chromatography-Mass Spectrometry (GC-MS), X-ray Diffraction method (XRD), Field Emission Scanning Electron Microscope (FESEM), Energy Dispersive X-ray Analysis (EDAX), UV spectroscopy and photoluminescence. GC-MS analysis revealed a single hit compound and eight hit compounds from the leaf and stem extracts. Also, the *in silico* molecular docking of these target compounds was performed with Caspase-9, TNF-alpha, HER-2 and ER-alpha receptor proteins to validate the best binding affinity poses. The ability of the target compounds from the leaf and stem extracts to bind to receptor proteins shows that they can stop cell growth, as shown by the higher binding energy values. **Results:** The XRD data affirms the peak formation at a 2θ value of 38.86º, which is attributed to the lattice plane at (111). FESEM images validate the shape and structure of leaf-AgNPs and stem-AgNPs, respectively, upon analysis. UV spectrophotometric analysis reveals the surface plasmon resonance peaks of AgNPs. Photoluminescence peaks were observed at 449 nm by the leaf-AgNPs and 449 nm and 504 nm by the stem-AgNPs were documented. The ABTS assay is performed to evaluate the antioxidant effect of AgNPs. Also, the antiproliferative effect of AgNPs was determined by MTT assay at several concentrations from 1.95 µg/mL to 250 µg/mL in the MCF-7 cancer cell line. **Conclusion:** The remarkable results suggest that AgNPs could be explored further as a therapeutic agent in pharmacological applications.

Keywords: Silver nanoparticles, GC-MS, Autodock Vina, FESEM, MCF-7, *Canavalia rosea*.

Correspondence:
Mrs.Vasanthi R
PG and Research, Department of Biotechnology, Sri Vinayaga College of Arts and Science (Affiliated to Thiruvalluvar University, Serkkadu, Vellore-632115), Ulundurpet, Tamil Nadu, INDIA.
Email: vasuramphd@gmail.com

Received: 11-03-2024;
Revised: 02-05-2024;
Accepted: 03-06-2024.

INTRODUCTION

Nanotechnology, an emerging indispensable tool, is involved in various biotechnological approaches. Industrial sectors like food, pharmaceuticals, electronics, home appliances, skincare supplies, textiles and agriculture have progressed through applied nanotechnology. Due to their small size, the nanoparticles provide significant physico-chemical and biological attributes.[1] Synthetic methods are followed in constructing nanoparticles but they pose deleterious effects like handling perilous chemicals, elevated temperature and pressure for processing and discharge of toxic derivatives.[2,3] Researchers reported an alternative approach for synthetic methods: green synthesis processes. Biogenic methods are well-suited as they are eco-friendly, less toxic, easy to accomplish, reliable and economical.[4-6] Diverse sources like bacteria, plants, algae, diatoms, actinomycetes, yeast and fungi were targeted as catalysts in nanoparticle synthesis.[7]

Metals like copper, gold, zinc, silver, magnesium, cobalt, selenium, palladium and ruthenium were involved in generating nanoparticles. Amidst these metals, silver nanoparticles are prevalent, as they exhibit astounding properties, viz., antimicrobial, anticancer and antioxidant.[8] Silver remains in its dormant state, whereas it gets ionized once combined with the moisture in wounds. The proactive silver ion sequesters tissue proteins and precedes morphological alterations in the bacterial cell wall and nuclear membrane, which eventually result in cell deformation and lysis.[9,10]

Plant extracts are extensively used for AgNP synthesis, as they are abundant in phytochemical fractions and efficient in reducing silver ions. The phytochemical fraction includes polyphenols, tannins, flavonoids, terpenoids, polysaccharides, etc.[11,12] The phytochemical analysis of the methanolic leaf and stem extract of *C. rosea* revealed the presence of alkaloids, cardiac glycosides, tannins, flavonoids, phytosterols, phlobatannins, saponins,

DOI: 10.5530/ijper.58.3s.95

Copyright Information :
Copyright Author (s) 2024 Distributed under Creative Commons CC-BY 4.0

Publishing Partner : EManuscript Tech. [www.emanuscript.in]

steroids, xanthoproteins and terpenoids.[13] The focus of this study is the synthesis, characterization and antiproliferative efficiency of silver nanoparticles using leaf and stem extracts of *Canavalia rosea*, a coastal dune plant. This is the first study to report the synthesis of silver nanoparticles from this plant. Many beans from Coastal Sand Dunes (CSD) on the west coast of India can be used as green manure, mulch, cover crops, feed, pasture beans, oil production and medicinal value.[14] The plant possesses remarkable medicinal attributes, which are evident from the previous experiments conducted using this plant.[15-17]

MATERIALS AND METHODS

Collection and preparation of plant extracts

A *Canavalia rosea* sample was collected from the coastal area of Cuddalore district, Tamil Nadu, India. The leaf and stem samples from the plant were dried, powdered and stored in an airtight container. The 10 g of leaf and stem powder was diffused in 100 mL of methanol in an Erlenmeyer flask. The mixture was warmed for 20 min at 60ºC and the flask was incubated at room temperature in a dark area for 24 hr. The supernatant from the solution is drained using Whatmann filter paper No. 1 in a sterile beaker. The filtered extract was used fresh for additional assays.

GC-MS analysis of *C. rosea* leaf and stem extracts

Using GC-MS analysis, the bioactive components in *C. rosea* leaf and stem extracts were evaluated. Briefly, the oven temperature was adjusted to 300ºC for the GC study, 200ºC for the ion source and 36.5 cm s^{-1} for the transfer line. Helium was used as the carrier gas, with a split ratio of 1:40, ionization energy of 70 eV, a scan range of 40-400 u and a scan time of 1 s (Adams 2007). After mixing 1 mL of hexane with the crude *C. rosea* leaf and stem extracts, it was filtered through a nylon filter. The 0.7 aliquot was put into a mass spectrometer-equipped chromatogram in split-less mode (Agilent, USA). For separation, the fused silica capillary column was employed. The 40-650 amu range was intended for scanning by the sector mass analyzer. The extract's volatile components were identified through the use of spectral data and computer-assisted matching with the NIST library.[21,30]

Green synthesis of silver nanoparticles from leaf (Leaf-AgNPs) and stem extract (Stem-AgNPs)

1 mM $AgNO_3$ is used as the substrate to prepare NPs. The leaf and stem extracts were blended with a silver nitrate solution. The concoction is heated at 60ºC in a magnetic stirrer for an hour. The solution's transformation from green to brown confirmed the reduction of Silver Ions (Ag+) to AgNPs (Ag0). The suspension is now transferred to a hot air oven and incubated for 4-5 hr at 100-150ºC. The dry residue was scraped using a sterile spatula and the parched powder of AgNPs from both extracts was stored in sterile Eppendorf tubes.[18]

Characterization of the synthesized AgNPs

The phytochemical constituents of the Le-AgNPs and Se-AgNPs were determined by gas chromatography-mass spectrometry using GCMS (Clarus 680 model, PerkinElmer). The structural characterization of the synthesized nanoparticles (Le-AgNPs and Se-AgNPs) was determined by the X-ray diffraction method using SHIMADZU-6000 by applying monochromatic Cu-Kα radiation and a wavelength range of 1.5406Å. The XRD patterns were documented in 2θ intervals from 10º to 90º with steps of 0.05º at room temperature. FESEM analysis, along with EDX analysis, is performed using a ZEISS-SIGMA microscope to interpret the surface morphology of nanoparticles and the elemental composition of the fabricated AgNPs, respectively. The JASCO V-670 spectrophotometer is used to infer the optical absorption spectrum, which is in the range of 0-1200 nm. The Photoluminescence spectrum (PL) was observed at room temperature using Prolog 3-HORIBAJOBINYVON at an excitation wavelength of 375 nm.

Molecular docking

Preparation of ligands

The GC-MS analysis revealed leaf-AgNPs describing one sharp peak in chromatogram which corresponds to 3-methyl-D-glucose, whereas Stem-AgNPs resulted in 8 major peaks in the chromatogram corresponding to namely cathinone, asparagine DL, oxaloacetic acid, N-seryl serine, ethanol-2-(1-methyl ethoxy)-acetate, N-acetyl-D-serine, 1,2-hydrazine carboxamide, propane dioic acid and propyl. These bioactive compounds, presenting strong influential peaks were preferred for the docking analysis, as all of these followed "Lipinski's rule of 5". This rule of 5 recommends the absorption or permeation of a drug molecule or its oral intake is feasible only when the following conditions are monitored[19] (Benet *et al.*, 2016):

i) Hydrogen Bond Donors (HBD) not more than 5.

ii) H-Bond Acceptors (HBA) not more than 10.

iii) Molecular weight (Mol.wt.) not more than 500.

iv) Octanol-water partition coefficient (Log P) not more than 5.

The PubMed database is directed to download these compounds (from the leaf-AgNPs and Stem-AgNPs) in SDF format (.sdf) and then transformed to PDB format (.pdb) with the help of Open Babel GUI software (version 2.3.1)[20,21] (Kim 2021; O'Boyle *et al.*, 2011). Table 1 shows the selected phytocompounds with their PubChem IDs and properties. These selected ligands were prepared using Autodock Tools (ADT) 1.5.7 before the docking procedure[22] (Morris *et al.*, 2009). The ligands were processed by defining their roots, designating hydrogen atoms and aromatic carbons, torsion numerals, the addition of gasteiger charges and saved in pdbqt format.

Protein Preparation

The receptor proteins specific to breast cancer were assigned for analysis by retrieving the three-dimensional structures of the protein sequences from the Research Collaboratory for Structural Bioinformatics (RCSB) Protein Data Bank (https://www.rcsb.org/) in PDB format. The proteins selected for the analysis are caspase 9 (PDB ID: 1NW9, Resolution: 2.40Å)[23] (Figure 3) (Shiozaki *et al.*,2003), estrogen receptor (PDB ID:1A52, Resolution: 2.80Å)[24] (Figure 4) (Tanenbaum *et al.*,1998), tumor necrosis factor (PDB ID:1TNF, Resolution: 2.60Å)[25] (Figure 5) (Eck and Sprang,1989) and human epidermal growth factor (PDB ID:3PP0, Resolution: 2.25Å)[26] (Figure 6) (Aertgeerts *et al.*,2011), corresponding to the PDB IDs 1NW9, 1A52, 1TNF and 3PP0, respectively. The protein file was downloaded as (.pdb file) and opened in ADT 1.5.7 for its preparation before docking. Also, the water molecules and heteroatoms are removed, with the addition of polar hydrogens to the target protein. Sequentially, the protein was assigned with Kollman charges and saved in pdbqt format.

Docking procedure

The bioactive compounds from leaf-AgNPs and Stem-AgNPs were docked against all four proteins selected to evaluate their binding interactions. We performed a blind docking procedure using Autodock Vina software. The target protein was fixed in a rigid position by applying the Lamarckian genetic algorithm and Monte Carlo simulated annealing. The amino acids in the binding sites were chosen and the grid box was created with the help of an auto grid. The X, Y and Z dimensions were set as 56×48×52 Å points, grid spacing at 1Å and grid box covering the whole protein (X centre=28.098, Y centre=34.923, Z centre=26.723). The GA runs were set to 50 and the population size was fixed at 300. Other GA parameters were fixed with default values. The binding interactions of the phytocompounds with the proteins were determined based on the high negative values, enabling the ranking of docked ligands. The visual representation of the interactions between the receptor and ligand molecule was represented by The Discovery Studio 2021 software.

In vitro analysis

ABTS Inhibition Assay

The antioxidant activity of the AgNPs was analyzed using an ABTS assay.[27] ABTS (2,2 azino bis (3-ethylbenzothiazoline-6-sulphonic acid) diammonium salt) was made by combining 5 mL of (7 mM ABTS) and 88 µL of 140 mM potassium persulfate. This step is carried out in the dark and at room temperature for 16 hr. This solution was diluted with 50% ethanol and the OD value was recorded at 734 nm. The assay was performed with 5 mL of this ABTS solution and 0.1 mL of extract at four different concentrations (31.25, 61.25, 125 and 250 µg/mL). The final absorbance values are read at 743 nm.

$$\text{Percentage of Scavenging}=[[A_o-A_1]/A_o]x100$$

The above formula has been used to calculate the percentage of radical scavenging activity, where A_o and A_1 are the absorbance values of the control and the sample respectively.

MTT cytotoxicity assay

The cytotoxic effects of the synthesized AgNPs on the MCF-7 cells were evaluated using an MTT assay. Briefly, the MCF-7 cells (NCCS, Pune) at a concentration of $1x10^6$ cells/mL were cultured in a 96-well plate at 37°C for 24 hr. The cells were treated with AgNPs at varying concentrations ranging from 1.95-250 µg/mL. The absorbance values were determined at 570 nm after 72 hr of incubation and post-treatment with MTT.[28] Triplicate assays were

Table 1: Phytocompounds obeying Lipinski's rule of 5.

Sl. No.	Compounds	PubChem ID	Rotatable bonds	Mol. wt	HBD	HBA	LogP	TPSA
1.	3-O-methyl-D glucose	8973	6	194.18	4	6	2.9	107 Å
2	cathinone	62258	2	149.19	1	2	1.1	43.1 Å
3	Asparagine DL	236	3	132.12	3	4	3.4	106 Å
4	Oxaloacetic acid	970	3	132.07	2	5	0.6	91.7 Å
5	N-seryl serine	138784	5	192.17	5	6	4.9	133 Å
6	Ethanol-2-(1-methyl ethoxy)-acetate	87974	5	146.18	0	3	0.8	35.5 Å
7	N-acetyl-D-serine	10844522	3	147.13	3	4	1.2	86.6 Å
8	1,2 hydrazine carboxamide	8039	0	118.10	4	2	2.1	110 Å
9	Propane dioic acid, propyl	69037	3	146.14	2	4	0.9	74.6 Å

performed and the percentage cytotoxicity was calculated with the following formula:

$$\% \text{ Cell Viability} = \frac{\text{The optical density of the sample}}{\text{The optical density of the Control}}$$

Statistical analysis

The assays performed in this study were done in triplicates. One-way ANOVA analysis, followed by Tukey's test, is applied for the statistical data analysis. The existence of a significant statistical difference between the standard and AgNPs, with a *p* value (p=<0.001), was documented from the statistical test. The statistical analysis was performed using Graphpad Prism software (version 10.1.1).

RESULTS

GC-MS analysis

GC-MS analysis is one of the most influential techniques for the detection of the chemical constituents of plants.[29] The spectral ranges of the components were assessed with the spectral database of known components in the GCMS NIST library (2008).[30] TurboMass software version 5.4.2 is used for data analysis.

GC-MS analysis of leaf extract

The compounds detected from the GC-MS analysis of leaf extract include 17 compounds (including sorted compounds repeated several times) (Table 2). Amidst these compounds, compounds with strong and influential peaks were selected for the docking analysis, which sorts a single major compound from the leaf extract named 3-O-methyl-D-glucose (Table 2). Figure 1 displays the chromatogram of leaf extract.

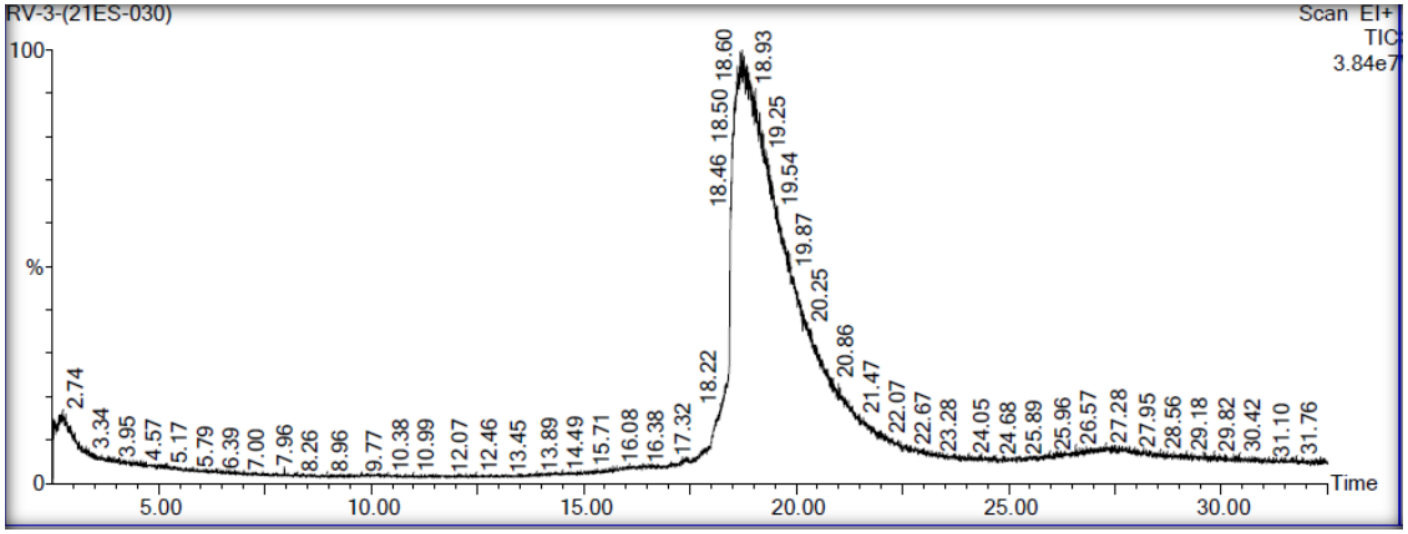

Figure 1: GC-MS Chromatogram of leaf extract.

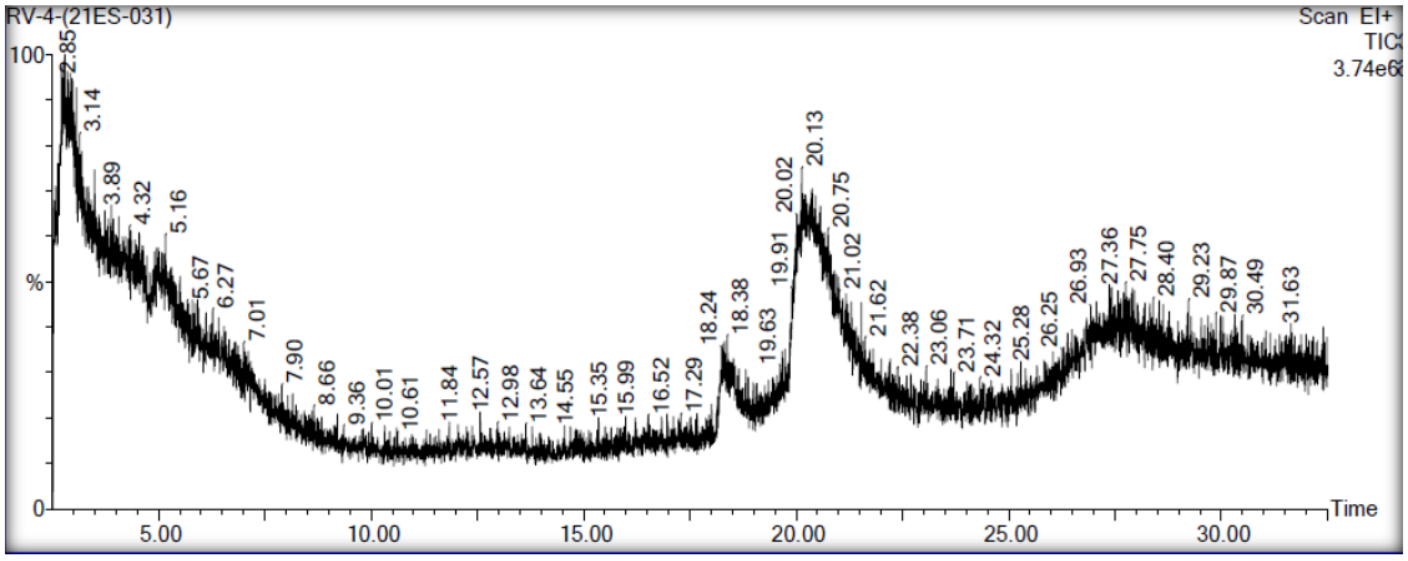

Figure 2: GC-MS analysis of stem extract.

GC-MS analysis of stem extract

The GC-MS analysis of stem extract displayed 81 compounds (including compounds repeated several times) (Figure 2). Similar to leaf extract, compounds showing predominant peaks were chosen for the docking analysis, comprising 8 leading compounds, namely cathinone, asparagine DL, oxaloacetic acid, N-seryl serine, ethanol-2-(1-methyl ethoxy)-acetate, N-acetyl-D-serine, 1,2-hydrazine carboxamide, propane dioic acid and propyl, as shown in Table 3.

Visual observation of AgNPs

The nanoparticle synthesis was initiated when the *C. rosea* leaf and stem extract were added to a 1 mM $AgNO_3$ solution. The $AgNO_3$ and *C. rosea* extract combination shows a color change from a green color to yellowish-green and later to a dark brown color, which evidences the formation of AgNPs.

Characterization of AgNPs

The assembly of AgNPs was further established by using X-ray diffraction, field emission scanning electron microscopy, EDAX analysis, UV spectroscopy and photoluminescence.

Molecular docking studies

The docking analysis was performed with the hit compounds obtained with Le-AgNPs and Se-AgNPs. There are 1 and 8 major compounds retrieved from both the Le-AgNPs and Se-AgNPs, respectively, which satisfy Lipinski's rule of 5. The autodock vina procedure validated the binding interactions of these phytochemical components with the selected proteins 1A52, 1TNF-, 1NW9 and 3PP0.

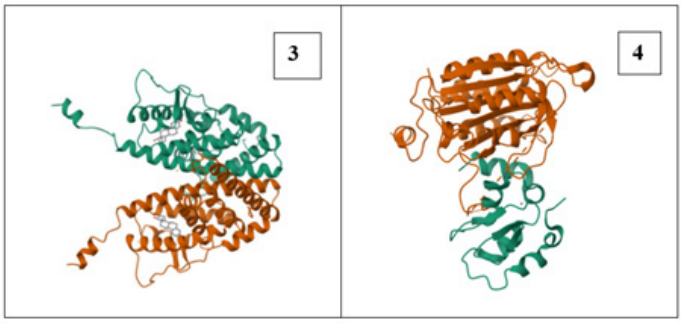

Figures 3 and 4: Structure of Caspase-9 (PDB ID 1NW9) estrogen receptor (PDB ID 1A52).

Molecular docking results of the Le-AgNPs

The binding interactions of 3-O-methyl-D-glucose were determined with the estrogen receptor, caspase-9, tumor necrosis factor-α and human epidermal growth factor. The proteins are represented by PDB IDs: 1A52, 1NW9, 1TNF-α and HER-2, respectively.

One covalent hydrogen bond at the Val 364 residue is observed with the estrogen receptor (1A52) (Table 4) (Figure 7A). This binding interaction showed a binding energy value of -3.7 kcal/mol. Three covalent hydrogen bonds at Ala22, Gly24 and Asp140 were noted with Tumor Necrosis Factor (1TNF-α) (Figure 7B). The binding energy established between (1TNF-α) and 3-O-methyl-D-glucose was -3.5 kcal/mol.

Three covalent bonds, Thr 308, Asp 309 and Gly 306 and one covalent-hydrogen bond, Lys 311, were detected with caspase-9 receptor protein (1NW9) (Figure 7C), respectively. The binding energy established between (1NW9) and 3-O-methyl-D-glucose was -4.1 kcal/mol. Also, with the human epidermal growth factor protein (3PP0), two covalent-hydrogen bonds are visualized at Lys 831 and Ser 834 residues (Figure 7D), exhibiting a binding energy value of -3.7 kcal/mol.

Molecular docking results of the Se-AgNPs

The docking analysis of stem extract AgNPs was performed with the 8 hit compounds with the selected proteins 1A52, 1NW9, 1 TNF-α and 3PP0. The binding interactions between the compound and the proteins were validated by the Autodock Vina procedure, as performed with leaf extract-AgNPs. The graphic representation of these binding interactions was displayed in Tables 5-8.

Binding interactions of compounds from Stem-AgNP with Estrogen receptor-α (1A52)

The stem extract-AgNPs produced eight hit compounds and these compounds exhibit binding interactions with the estrogen receptor-α and the specific binding modes of the individual compounds are addressed.

Cathinone forms a single covalent hydrogen bond with the estrogen receptor-α, with a binding residue of Leu 346. The best binding affinity was observed at -5.6 Kcal/mol between the protein and ligand; Figure 8(A) documents the binding interaction of

Table 2: Hit-Compound from GC-MS analysis of leaf extract.

Sl. No.	RT	Name	Structure	Mol. wt. (g/mol)	Mol. formula
1.	18.735	3-O-Methyl-D-glucose	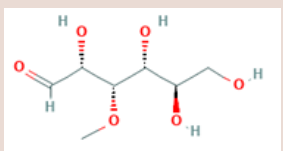	194	$C_7H_{14}O_6$

Table 3: Compounds identified from Stem extract+AgNPs.

Sl. No.	RT	Name	Structure	Mol.wt g/mol	Mol. formula
1.	18.375	Cathinone	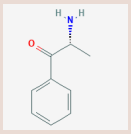	149	$C_9H_{11}ON$
2.	19.905	Asparagine DL	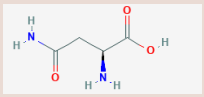	132	$C_4H_8O_3N_2$
3.	20.105	Oxaloacetic acid	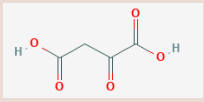	132	$C_4H_4O_5$
4.	20.130	N-Seryl Serine	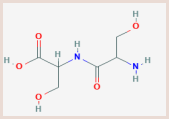	192	$C_6H_{12}O_5N_2$
5.	20.155	Ethanol-2-(1-methylethoxy)-acetate		146	$C_7H_{14}O_3$
6.	20.381	N-acetyl-D-Serine	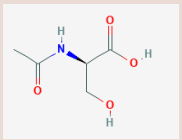	147	$C_5H_9O_4N$
7.	20.461	1, 2- hydrazine carboxamide	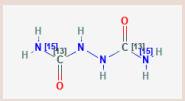	118	$C_2H_6O_2N_4$
8.	20.671	Propane dioic acid, Propyl.	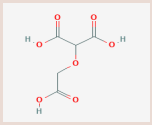	146	$C_6H_{10}O_4$

this compound. Asparagine establishes four covalent hydrogen bonds with repeating residues at the Asp332 and Ser341 residues. The best binding affinity was recorded at -4.6 kcal/mol, which is shown in Figure 8(B). Oxaloacetic acid generates three binding interactions with estrogen receptor-α, with binding residues Leu 346, Glu 353 and Arg 394. The binding energy observed with this interaction was -4.5 kcal/mol, as displayed in Figure 8(C). N-Seryl serine forms two covalent hydrogen bonds with the residues Ser 329 and Tyr 331, with a binding energy of -5.3 Kcal/mol, with the estrogen receptor Figure 8(D). Ethanol-2-(1-methylethoxy)-acetate showed two covalent hydrogen bonds at Asp 332 and Arg 335 residues, with a binding energy of -3.7 Kcal/mol, as shown in Figure 8(E). N-acetyl-D-serine presented a single covalent hydrogen bond with the estrogen receptor at the Thr 465 residue, with a binding energy value of -4.0 Kcal/mol, as portrayed in Figure 8(F). 1,2-hydrazine carboxamide posed a single covalent hydrogen bond with the estrogen receptor at the Asp332 residue, with a binding energy value of -6.1 Kcal/mol, as portrayed in Figure 8(G). Propane dioic acid, propyl, exhibited a single covalent hydrogen bond interaction at Lys 481 residue. Also, this compound forms two carbon-hydrogen bonds with Lys 481 residue. The binding energy recorded in this interaction was -5.1 kcal/mol Figure 8(H).

Binding interactions of compounds from Stem-AgNP with Caspase 9 protein (1NW9)

Cathinone and asparagine DL generate two covalent hydrogen bonds each, with Arg268, Arg286 and Thr274, Thr271, respectively, corresponding to binding energies of -4.7 and -3.8 kcal/mol (Figure 9A and B). Oxaloacetic acid showed a binding affinity of -4.0 kcal/mol by forming five covalent-hydrogen bonds at Gln319, Glu318, His346, Thr345 and Ile342 residues (Figure 9C). N-seryl serine binds effectively at Tyr265 and Arg268 residues with an energy binding value of -6.2 kcal/mol (Figure 9D). Ethanol-2-(1-methyl ethoxy)-acetate makes effective binding at two residues of Gln319, forming a covalent-hydrogen bonding pattern. The binding energy was measured to be -2.9 kcal/mol, as shown in (Figure 9E). Two covalent hydrogen bonds were

formed by the N-acetyl-D-serine at Gln319 residues, initiating an energy value of -3.5 kcal/mol of binding (Figure 9F). Similarly, 1,2 hydrazine carboxamide establishes two covalent hydrogen bonds with Thr271 and Ala291 residues, creating binding energy of -4.5 Kcal/mol (Figure 9G). The final compound, propane dioic acid, propyl, forms three covalent hydrogen bonds at the Arg268, Tyr265 and Trp317 residues, producing a binding energy value of -6.2 kcal/mol. Also, it forms one carbon-hydrogen bond at the Arg286 residue (Figure 9H).

Binding interactions of compounds from Stem-AgNP with tumor necrosis factor-α (1TNF-α)

Cathinone establishes a single covalent-hydrogen bond with the binding residue Gln102. The interaction between the protein and the ligand exhibits the best binding affinity at -3.9 kcal/mol, as shown in Figure 10(A). Asparagine forms three covalent hydrogen bonds and one carbon-hydrogen bond, with Pro113, Lys112, Cys69 and Gly68, respectively. The best binding affinity with the covalent-hydrogen bond interaction was -3.6 kcal/mol. Figure 10(B) represents the binding interactions of asparagine DL with 1TNF-α. Oxaloacetic acid creates the finest binding affinity, with a binding energy of 4.2 kcal/mol, forming four covalent hydrogen bonds with Glu135, Lys90, Thr79 and Thr77 residues, as depicted in Figure 10(C). N-Seryl Serine forms two bonds, as shown in Figure 10(D), one covalent hydrogen bond and one carbon-hydrogen bond at Arg103 and Lys112 residues, respectively. Ethanol-2-(1-methyl-ethoxy)-acetate forms a single covalent-hydrogen bond with a binding energy of -2.8 Kcal/mol at the Thr77 residue, as indicated in Figure 10(E). Similarly, compounds N-acetyl-d-serine and 1,2 hydrazine carboxamide established a single covalent hydrogen bond with binding affinity -3.9 and -5.0, respectively, at the corresponding residues, Pro 139 and Gln102, as given in Figure 10(F and G). Two covalent-hydrogen bonds are formed by propane dioic acid propyl at Tyr59 and His15 residues, with a binding energy of -5.8 kcal/mol Figure (10H).

Binding interactions of compounds from Stem-AgNPs with Human Epidermal Growth factor-2 (3PP0)

Cathinone forms two covalent hydrogen bonds with Arg756 and Gly729 residues, with a binding energy value of -4.4 Kcal/mol (Figure 11A). Asparagine DL showed four covalent hydrogen bonds with Thr862, Asn850, Thr862 and Ser728 residues, with a binding energy value of -4.2 Kcal/mol. Also, it forms a single carbon-hydrogen bond at the Gly68 residue (Figure 11B). Oxaloacetic acid forms two covalent hydrogen bonds at the Glu770 and Gly865 residues (Figure 11C). A binding energy

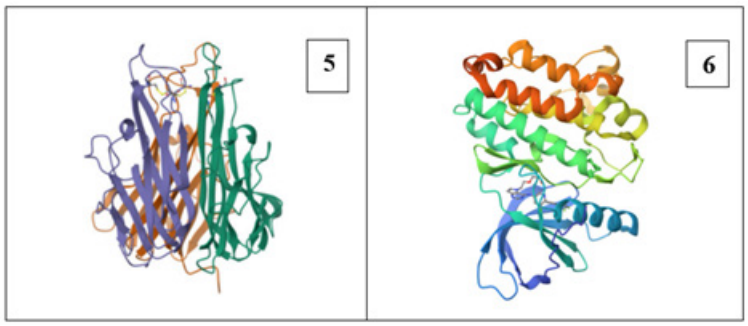

Figures 5 and 6: Structure of Tumor Necrosis factor (PDB ID TNF-α) and Human Epidermal Growth factor (PDB ID 3PP0).

Table 4: Docking analysis of leaf extract + AgNPs and interpretation of binding interactions between 3-O-methyl-D-glucose (hit compound from Leaf - AgNP) with various protein targets 1A52, 1TNF-α, 1NW9 and 3PP0.

Sl. No.	Compound	Docked Protein	Binding energy	conventional Hydrogen bonds		Carbon-Hydrogen bond	
1.	3-O-methyl-D-glucose	1A52	-3.7	1	Val364	-	-
2.		1TNF -α	-3.5	3	Ala22 Gly24 Asp140	-	-
3.		1NW9	- 4.1	3	Thr308 Asp309 Gly306	1	Lys311
4.		3PP0	-3.7	2	Lys831 Ser834	-	-

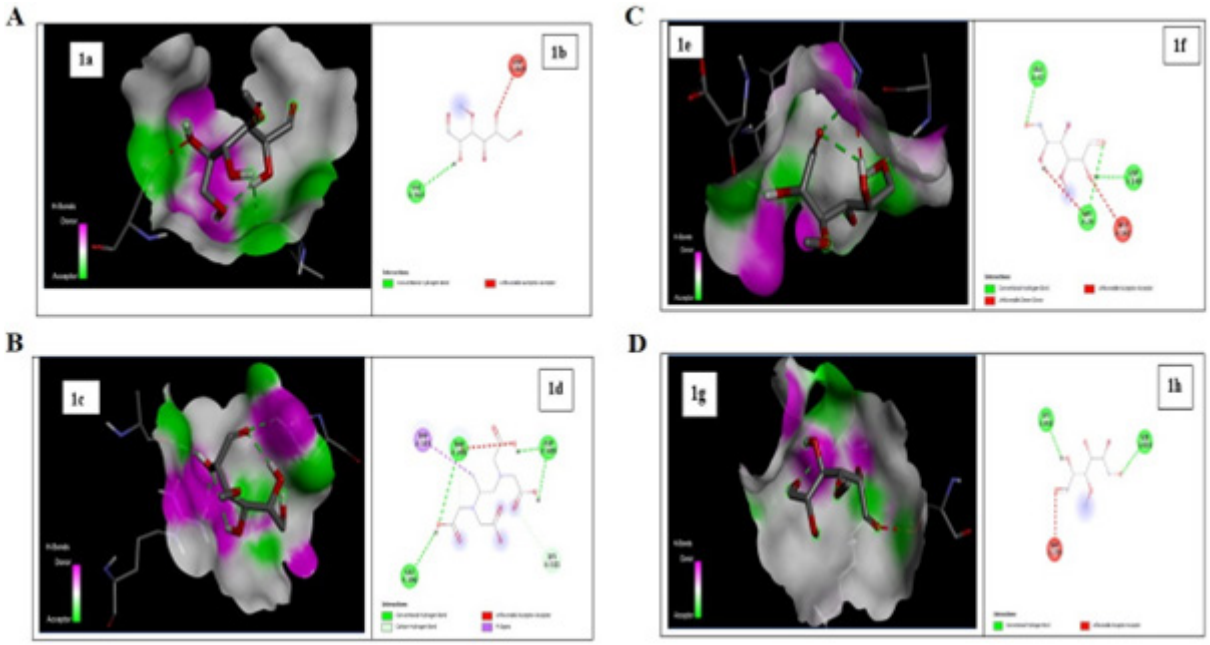

Figure 7: Molecular interactions of 3-O-Methyl-D-glucose with estrogen receptor (A), caspase-9 (B), tumor necrosis factor (C) and human epidermal growth factor-2 (D).

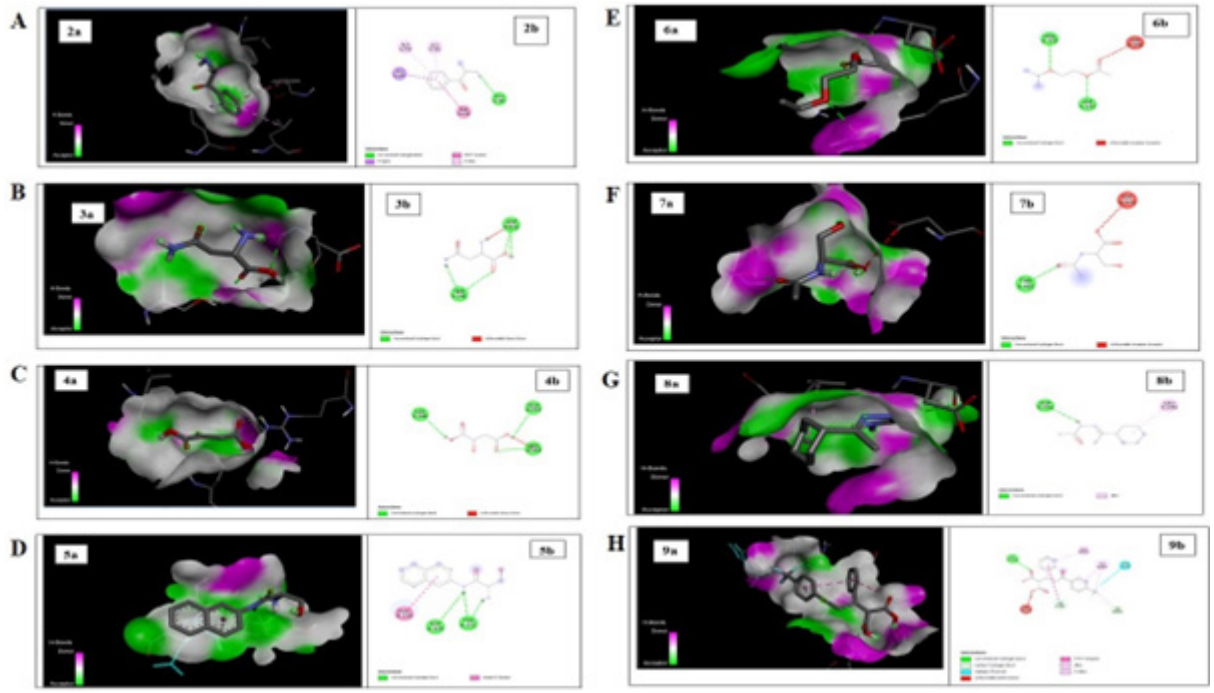

Figure 8: Molecular interactions of estrogen receptor-α (PDB ID:1A52) with cathinone (A), asparagine DL (B), oxaloacetic acid (C), N-seryl serine (D), ethanol-2-(1-methylethoxy)-acetate (E), N-acetyl-D-Serine (F), 1,2-hydrazine carboxamide (G) and propane dioic acid, propyl (H) molecules.

value of -4.2 kcal/mol was noted for the above ligand interaction. N-Seryl serine establishes one covalent-hydrogen bond and two carbon-hydrogen bonds at Ser728, Asn850 and Asp863 residues, respectively (Figure 11D). The binding energy generated with the above covalent-hydrogen bonding was found to be -5.2 kcal/mol. Ethanol-2-(1-methyl ethoxy)-acetate generates two carbon-hydrogen bonds with a binding energy value of -2.8 kcal/mol (Figure 11E). No covalent-hydrogen bond was generated with this compound. N-Acetyl-D-Serine generates one covalent hydrogen bond and one carbon-hydrogen bond with a binding energy value of -3.9 kcal/mol (Figure 11F). Unlike the other compounds, 1,2 hydrazine carboxamide and propane dioic acid propyl generate a greater binding value of -5.7 Kcal/mol (Figure 11G and H). 1,2 hydrazine carboxamide binds with one covalent

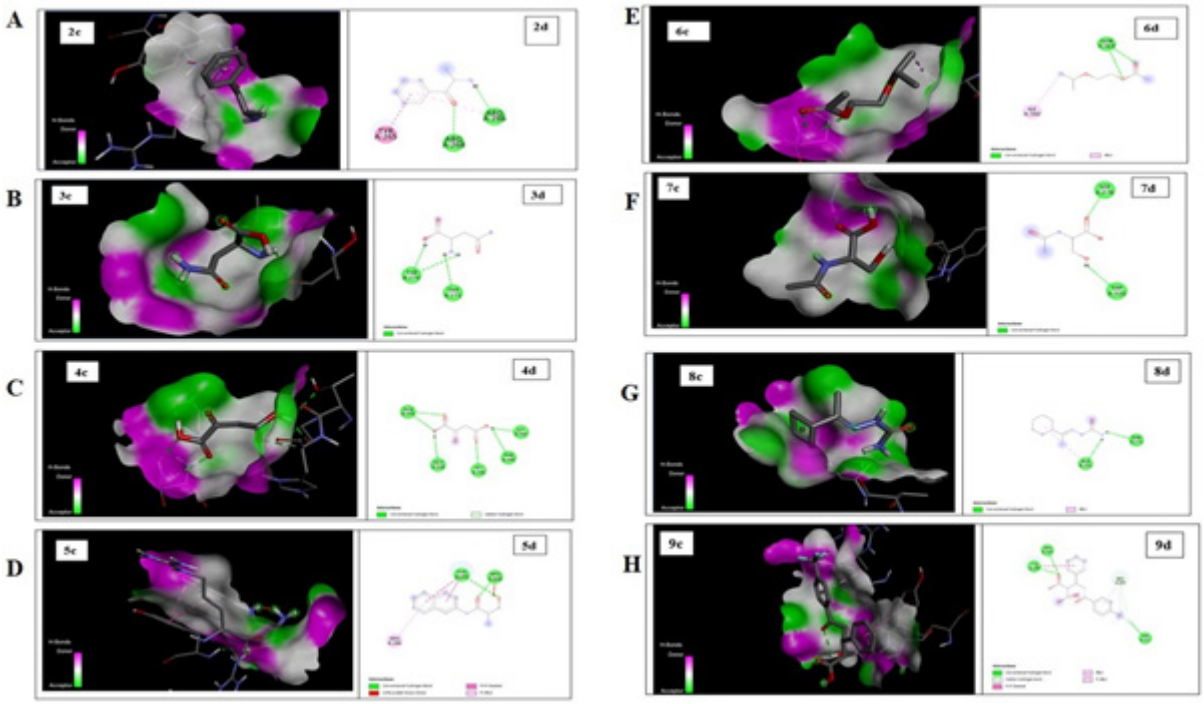

Figure 9: Molecular interactions of Caspase-9 protein (PDB ID:1NW9) with cathinone (A), asparagine DL (B), oxaloacetic acid (C), N-Seryl Serine (D), Ethanol-2-(1-methylethoxy)-acetate (E), N-Acetyl-D-Serine (F), 1,2-hydrazine carbamide (G) and propanedioic acid, propyl (H) molecules.

hydrogen bond at the Glu 766 residue, whereas propane dioic acid, propyl, doesn't generate a covalent hydrogen bond but forms three carbon-hydrogen bonds at the Pro945, Thr917 and Pro942 residues.

XRD analysis

An X-ray diffraction pattern was able to determine the crystalline nature of the biosynthesized AgNPs. XRD reveals the shape and size of AgNPs from leaf and stem extracts. The pattern of XRD discloses the definite and clear Bragg reflections with values of 28.7º, 33.1º, 39º, 45.1º, 65.3º and 78.4º at 2θ, which are indexed to the 210, 122, 111, 200, 220 and 311 planes of a faced center cubic lattice of silver (correlating to ICDD-JCPDS card number 04-0783). The most prominent peak occurred at a 2θ value of 38.86◦ and was attributed to the lattice plane at (111). The peak indexed as (111) in the XRD pattern suggests the better fabrication of nanoparticles (Figure 12). The intense peaks of the XRD pattern reflect the crystallinity of the nanoparticles. Besides, the diffraction peaks obtained were small, which implies that the crystal size is remarkably small.

FESEM and EDAX analysis

Figure 13(A) demonstrates the FESEM images of the AgNPs synthesized from the leaf extract, enabling the depiction of the shape, size and nature of the distribution of the synthesized silver nanoparticles. AgNPs from both extracts are rod-shaped and cylindrical in shape, forming a mat-like structure due to the aggregates of nanoparticles, which is a general characteristic feature of nanoparticles synthesized from plant extracts biologically. The EDAX spectrum of AgNPs is represented in Figure 13(B).

UV Analysis

Figure 14 illustrates the UV-absorption spectra of the synthesized AgNPs, which show the nanoparticles were formed once the reaction was initiated. The UV plot graph of leaf extract with AgNPs showed a shift in absorbance peak at 289 nm. The stem extract with AgNPs also exhibits an absorbance peak at the same 289 nm.

Photoluminescence

The green synthesized AgNPs were stated to display photoluminescence and their fluorescence spectra, as represented in Figure 15. The fabricated AgNPs synthesized from leaf extract were found to be luminescent at 449 nm, whereas the AgNPs from stem extract showed two emissions at 449 nm and 504 nm.

Antioxidant assay results

Figure 16 illustrates the ABTS assay results with the absorbance values recorded at 743nm. The leaf-AgNPs and stem-AgNPs showed a similar range of OD values when compared with the standard gallic acid. The gallic acid displayed 92%, 91%, 90% and 87% inhibition at 31.25, 62.5, 125 and 250 µg/mL. Leaf-AgNP demonstrates inhibition activity at a range of 85%, 84%, 83% and 82%, whereas stem-AgNP resulted in 80%, 78%, 76% and 75%

inhibition at the same test concentrations treated with standard (gallic acid).

MTT Assay

The recognition of antioxidant potential led us to investigate the effect of silver nanoparticles on the reduction of cell proliferation in the MCF-7 cell line through the MTT assay. The silver nanoparticles responded efficiently to reduce the proliferation of the MCF-7 cell line at lower concentrations. The AgNPs showed cellular membrane rupture and nuclear fragmentation in the treated cells. The assay was done at several concentrations ranging from 1.95, 3.9, 7.8, 15.6, 31.25, 62.5, 125 and 250 (µg/mL), as depicted in Figure 17. Leaf-AgNPs showed an inhibition range of 87%, 73%, 62%, 51%, 46%, 39%, 32% and 23% at the tested concentrations of silver nanoparticles, whereas stem-AgNPs displayed 97%, 89%, 78%, 72%, 66%, 52%, 42% and 38%. Figure 18 explains the IC_{50} values of both leaf-AgNPs and stem-AgNPs, which correspond to 9.23 and 24.3 µg/mL, calculated using GraphPad Prism Software 10.1.1.

Table 5: Docking analysis interpretation of binding interactions between hit compounds from Stem extract +AgNP with protein target 1A52 (estrogen receptor alpha protein).

Sl. No.	Compounds	Binding energy with protein 1A52	Covalent hydrogen bond		Carbon-hydrogen bond	
1	Cathinone	-5.6	1	Leu346	-	-
2	Asparagine DL	-4.6	4	Asp332, Ser341	-	-
3	Oxaloacetic acid	-4.5	3	Leu346, Glu353, Arg394	-	-
4	N-Seryl serine	-5.3	2	Ser329, Tyr331	-	-
5	Ethanol-2-(1-methylethoxy)-acetate	-3.7	2	Asp332, Arg335	-	-
6	N-acetyl-D-serine	-4.0	1	Thr465	-	-
7	1,2-hydrazine carboxamide	-6.1	1	Asp332	-	-
8	Propane dioic acid, propyl	-5.1	1	Lys481	2	His488 His501

Table 6: Docking analysis interpretation of binding interactions between hit compounds from Stem extract +AgNP with protein target 1NW9 (Caspase-9 protein).

Sl. No.	Compounds	Binding energy with protein 1NW9	Covalent hydrogen bond		Carbon-hydrogen bond	
1	Cathinone	-4.7	2	Arg268, Arg286	-	-
2	Asparagine DL	-3.8	2	Thr274, Thr271	-	-
3	Oxaloacetic acid	-4.0	5	Gln319, Glu318 His346, Thr345 Ile342	-	-
4	N-Seryl serine	-6.2	2	Tyr265, Arg268	-	-
5	Ethanol-2-(1-methylethoxy)-acetate	-2.9	2	Gln319	-	-
6	N-acetyl-D-serine	-3.5	2	Ser278, Trp310	-	-
7	1,2-hydrazine carboxamide	-4.5	2	Thr271, Ala291	-	-
8	Propane dioic acid, propyl	-6.2	3	Arg268, Tyr265 Trp317	1	Arg286

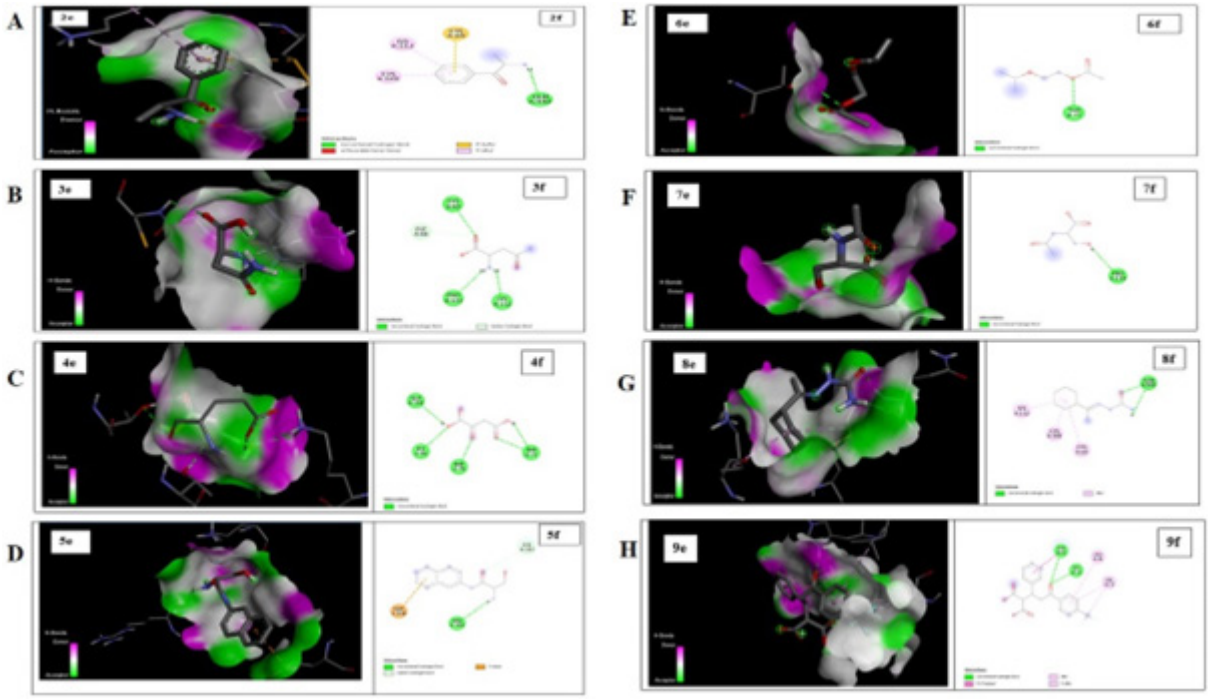

Figure 10: Molecular interactions of tumour necrosis factor (PDB ID:1TNF α) with cathinone (A), asparagine DL (B), oxaloacetic acid (C), N-Seryl Serine (D), Ethanol-2-(1-methyl ethoxy)-acetate (E), N-acetyl-D-Serine (F), 1,2 hydrazine carboxamide (G) and propanedioic acid, propyl (H) molecules.

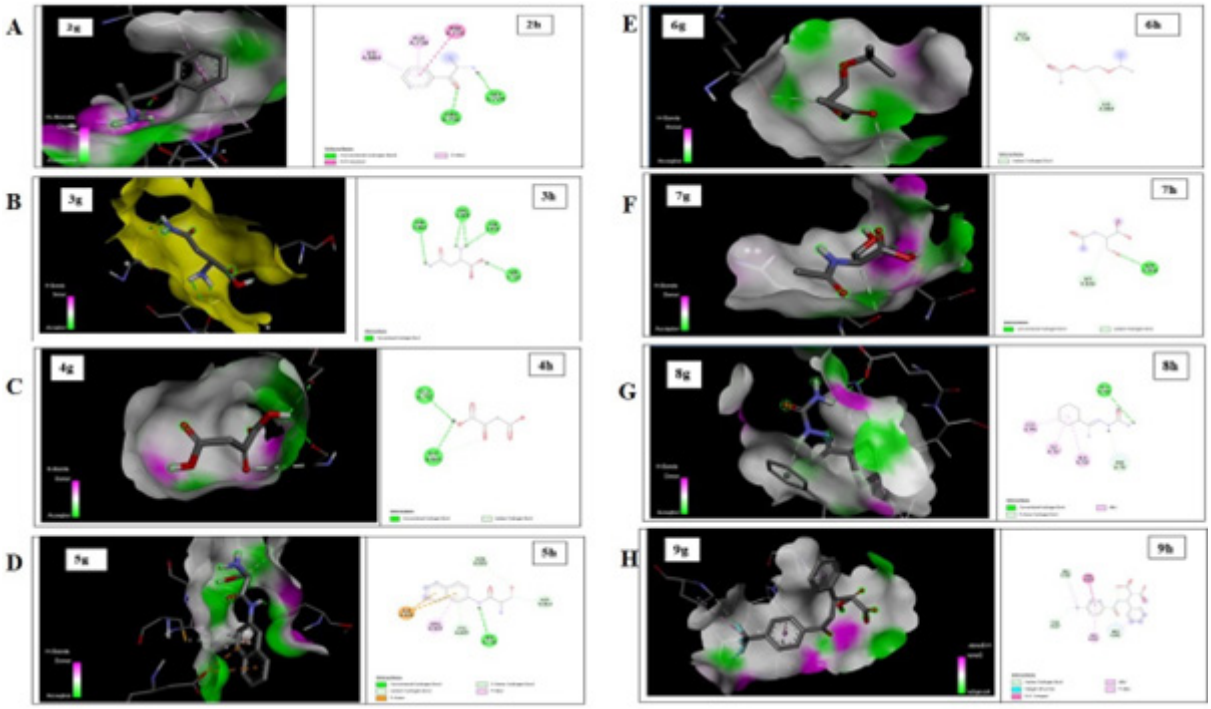

Figure 11: Molecular interactions of human epidermal growth factor-2 (HER-2- PDB ID:3PP0) with cathinone (A), asparagine DL (B), oxaloacetic acid (C), N-Seryl Serine (D), Ethanol-2-(1-methylethoxy)-acetate (E), N-acetyl-D-Serine (F), 1, 2-hydrazine carboxamide (G) and propanedioic acid, propyl (H) molecules.

DISCUSSION

Phytochemical analysis

A preliminary phytochemical analysis experimented with crude leaf extract of *C. rosea*, displayed the presence of tannins, phlobatannins, flavonoids, alkaloids, saponins, phenols and glycosides.[31] A similar study of phytochemical analysis of the seed extract of *Canavalia rosea* with petroleum ether extract

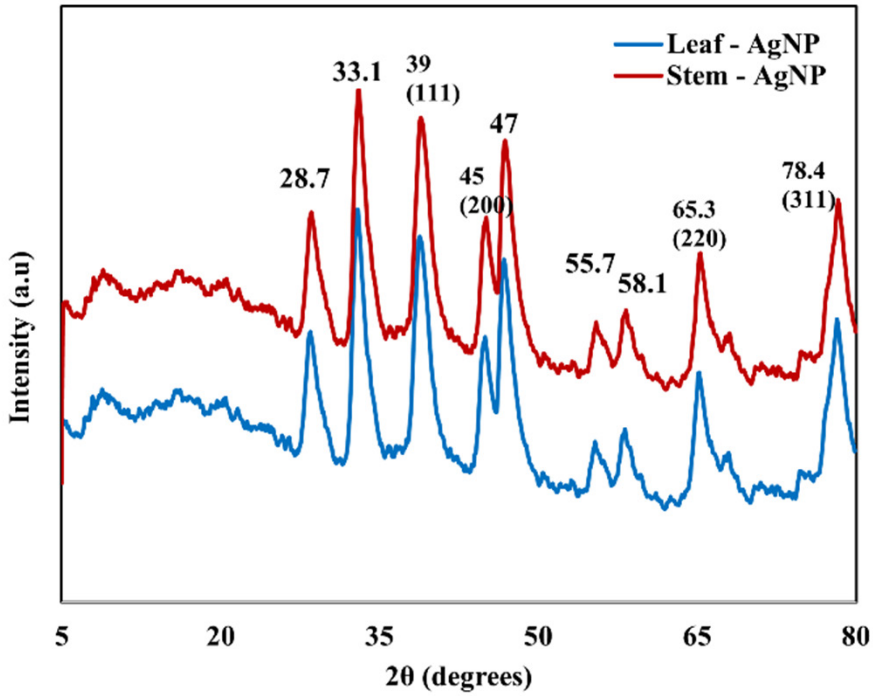

Figure 12: XRD analysis of the synthesized AgNPs.

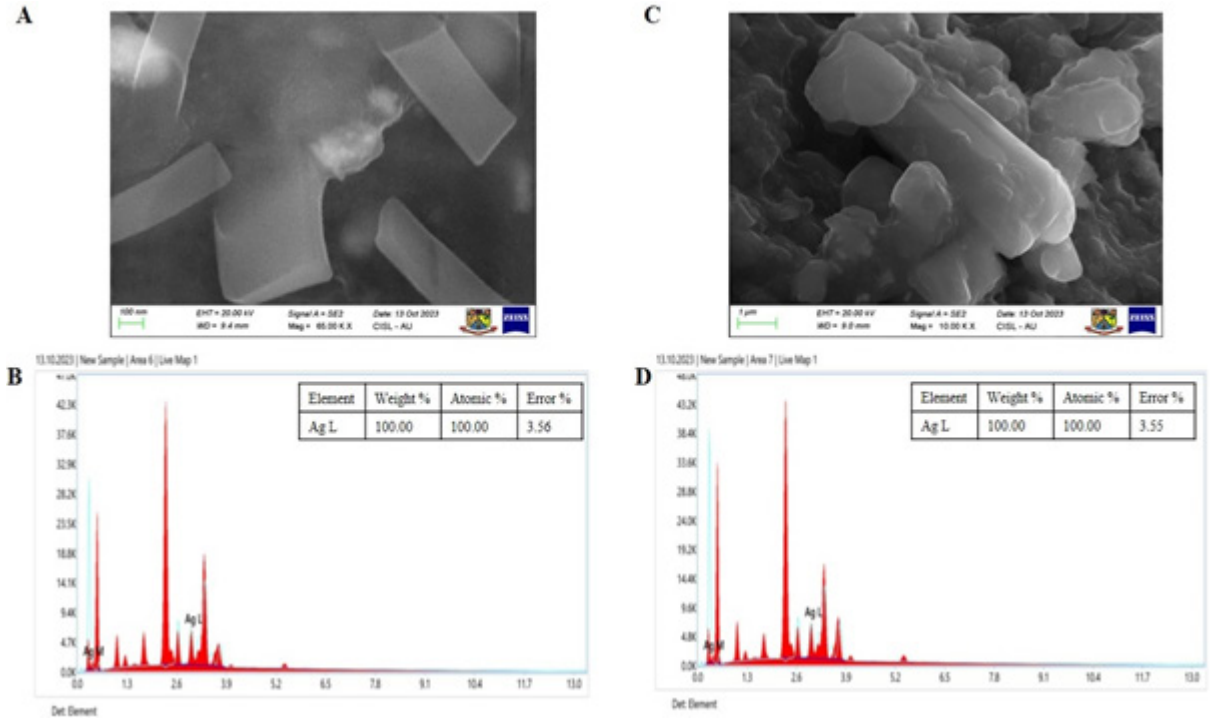

Figure 13: FESEM and EDAX analyses of the synthesized AgNPs.

was reported[32] by (Aswathi and Abdussalam, 2020). The study exposed eight major compounds namely tannins, saponins, flavonoids, cardiac glycosides, terpenoids, phenols, coumarins and phlobatannins. Similar results were documented in the phytochemical screening of *Canavalia rosea* leaf and stem extracts were carried out with five different solvents namely ethanol, distilled water, chloroform, acetone and methanol revealing the bioactive constituents such as alkaloids, terpenoids, phenolic compounds, flavonoids, tannins, etc.[13]

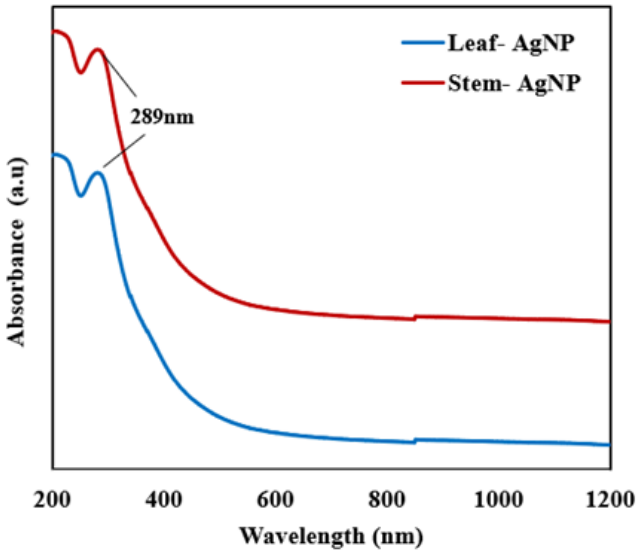

Figure 14: UV Spectrophotometric analysis of the synthesized AgNPs.

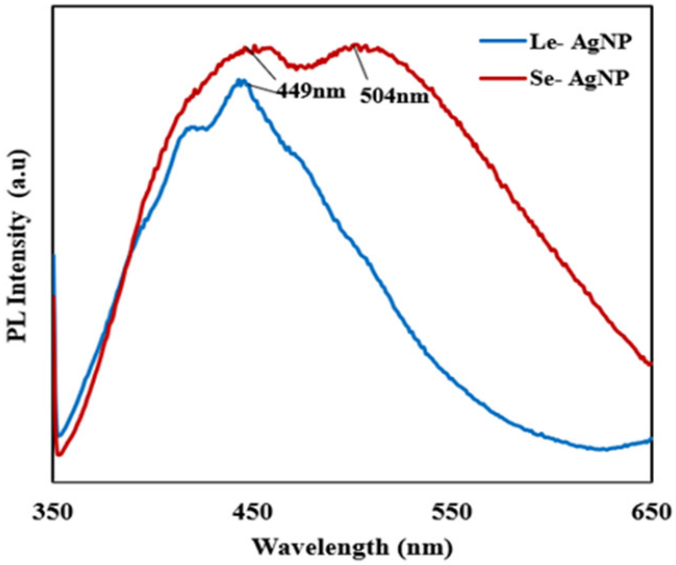

Figure 15: Photoluminescence analysis of the synthesized AgNPs.

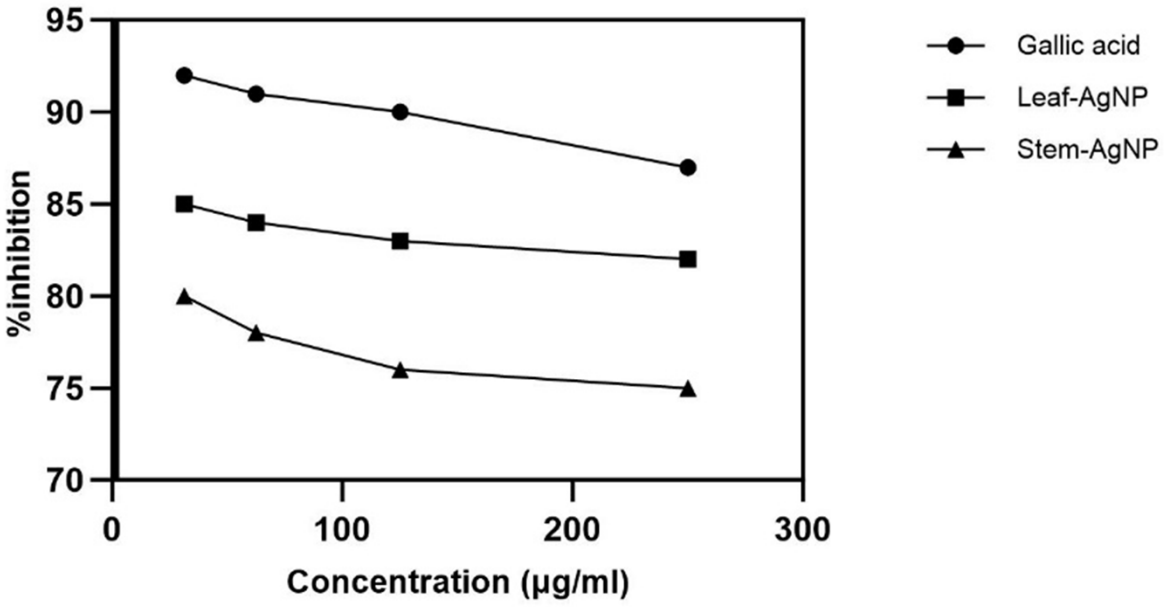

Figure 16: ABTS scavenging activity of the synthesized AgNPs.

The presence of such promising secondary metabolites impacts the antioxidant properties of *C. rosea*. Alkaloids and glycosides were part of pharmaceutical products, as an anesthetic agent and flavouring materials respectively,[33,34]. Additionally, flavonoids being a major part of the polyphenol group, influence the free radical scavenging property of the plants.[35]

Green synthesis of AgNPs

The transition of color from green to brown considered the initial step of confirmation of the fabrication of NPs, was facilitated by the secondary metabolites/phytoactive mixture, which further promotes the reduction of Ag ions. This color change is attributed to surface plasmon vibration, an optical property exclusive to noble metals.[36] The characterization of AgNPs plays a crucial role in the green synthesis method since physical parameters like shape, size and surface morphology affect their biological response. Additionally, the precursor used, incubation time, pH, incubation temperature, extract source and calcination temperature of NP synthesis determined the shape and size of the NPs.

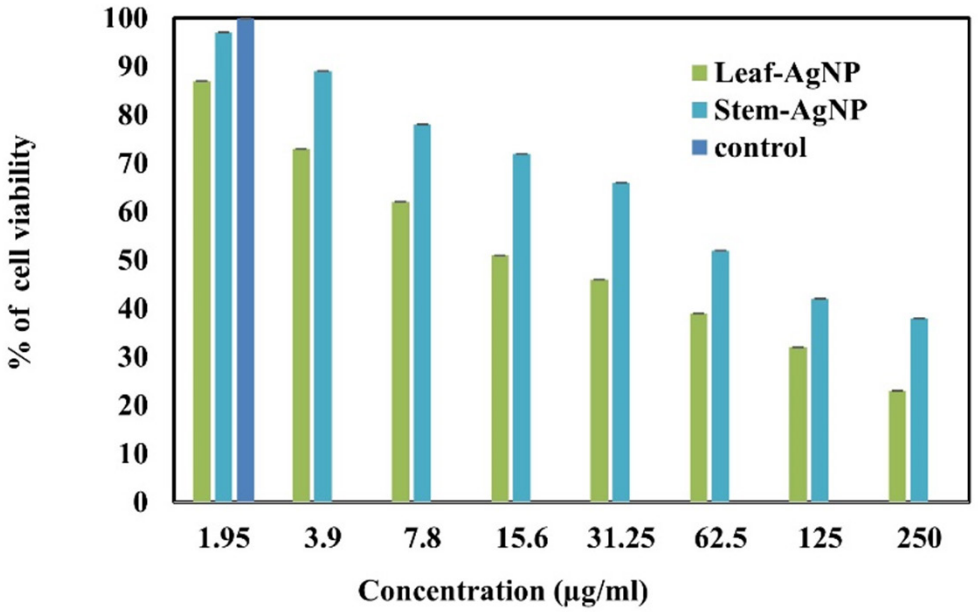

Figure 17: Cytotoxic activity of the synthesized AgNPs on the MCF-7 cells.

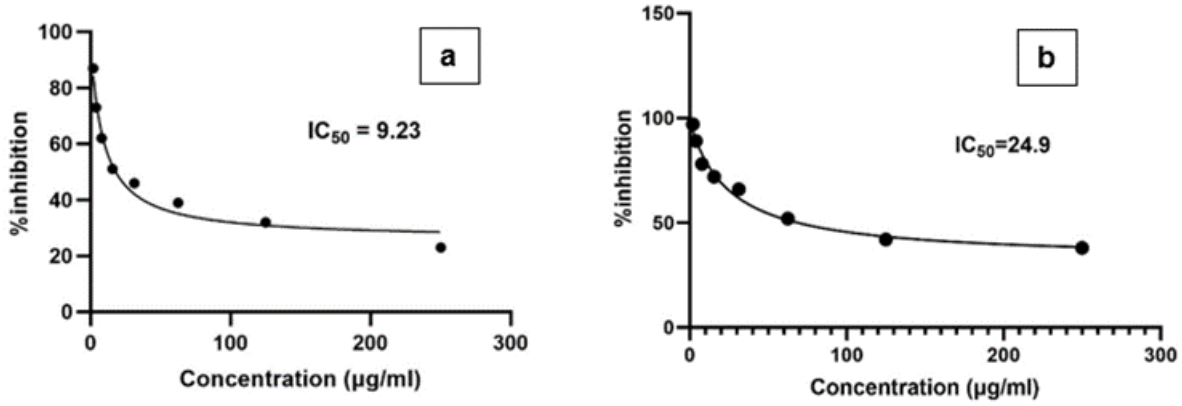

Figure 18: IC_{50} concnetrations of the synthesized AgNPs agaisnt the MCF-7 cells.

GC-MS study

Preliminary characterization of AgNPs was performed by GC-MS procedure, which reports the prevalent peaks representing the hit compounds from Leaf-AgNPs and Stem-AgNPs.

Docking analysis was performed with the AgNPs from both leaf and stem extracts. Among the binding interactions evaluated between the compound 3-O-methyl-D-glucose and protein targets, the highest binding energy value of -4.1 Kcal/mol was recorded for caspase-9 (PDB ID:1NW9). Both the estrogen receptor and human epidermal growth factor produced a binding energy value of -3.7 kcal/mol, which was slightly less than that exhibited by caspase-9. The binding energies suggest that the compound 3-O-methyl-D-glucose could be a source of antiproliferative properties against cancer cells.

3-O-methyl-D-glucose is a metabolically stable, chemical analog of glucose. This property of metabolic stability of the compound fits it to the exploration of cellular passage, blood-brain barrier and tissue distribution expanse of hexoses.[37] Likewise, recent studies suggest that 3-O-methyl-D-glucose has been utilized in the detection of malignancy progression.[38] The presence of 3-O-methyl-D-glucose in the GC-MS fraction of *Trigonella foenum* grecum was reported and the compound has a preservative

role.[39] Moreover, 3-O-methyl-D-glucose delivers considerable protection for the preservation of dried sperm at higher freezing temperatures devoid of rupturing cell membranes for biomedical purposes.[40]

A similar docking study with estrogen receptor-alpha, involving anticancer polyphenols from *Syzygium alternifolium*, confirmed them as potential ER-alleviating sources.[41] A related report on *in silico* analysis of ferulic acid with seven target proteins, including caspase 9 (PDB ID: 1NW9), revealed that ferulic acid could be a potent molecule with proapoptotic and anti-cell proliferative attributes.[42]

Among the docking interactions of Stem-AgNP with estrogen receptor alpha protein (1A52), 1,2 hydrazine carboxamide and cathinone resulted in the highest binding energy values -6.1 and -5.6Kcal/mol respectively. The Stem-AgNP compounds, propane dioic acid and N-seryl serine with Caspase-9 protein (1NW9)

Table 7: Docking analysis interpretation of binding interactions between hit compounds from Stem extract +AgNP with protein target 1TNF-α (Tumor necrosis factor alpha protein).

Sl. No.	Compounds	Binding energy with protein 1TNF-α	Covalent hydrogen bond		Carbon-hydrogen bond	
1	Cathinone	-3.9	1	Gln102	-	-
2	Asparagine DL	-3.6	3	Pro113, Lys112 Cys69	1	Gly68
3	Oxaloacetic acid	-4.2	4	Glu135, Lys90 Thr79, Thr77	-	-
4	N-Seryl serine	-4.6	1	Arg103	1	Lys112
5	Ethanol-2-(1-methylethoxy)-acetate	-2.8	1	Thr77	-	-
6	N-acetyl-D-serine	-3.9	1	Pro139	-	-
7	1,2-hydrazine carboxamide	-5.0	1	Gln102	-	-
8	Propane dioic acid, propyl	-5.8	2	Tyr59, His15	-	-

Table 8: Docking analysis interpretation of binding interactions between hit compounds from Stem extract +AgNP with protein target 3PP0 (Human epidermal growth factor).

Sl. No.	Compounds	Binding energy with protein 3PP0	Covalent hydrogen bond		Carbon-hydrogen bond	
1	Cathinone	-4.4	2	Arg756 Gly729	-	-
2	Asparagine DL	-4.2	4	Thr862, Asn850 Thr862, Ser728	-	-
3	Oxaloacetic acid	-4.6	2	Glu770, Gly865	1	Gly865
4	N-Seryl serine	-5.2	1	Ser728	2	Asn850 Asp863
5	Ethanol-2-(1-methylethoxy)-acetate	-2.8	-	-	2	Ala730 Lys883
6	N-acetyl-D-serine	-3.9	1	Ser834	1	Lys831
7	1,2-hydrazine carboxamide	-5.7	1	Glu766	-	-
8	Propane dioic acid, propyl	-5.7	-	-	3	Pro945 Thr917 Pro942

target produced -6.2Kcal/mol respectively, which are the highest binding energies. Propane dioic acid propyl with Tumor Necrosis Factor-alpha protein (1TNF-α) showed the greatest binding energy value of -6.2Kcal/mol. With human epidermal growth factor (3PP0), 1,2-hydrazine carboxamide and Propane dioic acid propyl displayed -5.7Kcal/mol as their highest binding energy values. These highest values of binding energy prove that these compounds could be the potential contributors of antioxidants, that neutralize the ROS species, thereby triggering cytotoxic pathways.

Docking analysis of carbohydrate-binding pockets in the lectin genes from various species of Canavalia (*C. virosa, C. pubescens* and *C. rosea*) was reported by (Nivetha *et al*., 2021).[43] Crude seed extract displayed the highest haemagglutination activity against buffalo RBCs. The study revealed that Asparagine (ASN), Serine (SER), Alanine (ALA), Valine (VAL), Tyrosine (TYR) and Threonine (THR) were the major residues associated with the binding of carbohydrates. Similar results were presented in our docking experiment, where the binding sockets of protein include amino acid residues such as asparagine, serine, alanine, valine, tyrosine and threonine along with proline, glycine, histidine, cystine, glutamine, tryptophan and isoleucine. This suggests that the recognition of these amino acids could be attributed to the biological efficiency of these silver nanoparticles.

Characterization of AgNPs

The characterization of AgNPs plays a crucial role in the green synthesis method since physical parameters like shape; size and surface morphology affect their biological response. Additionally, the precursor used incubation time, pH, incubation temperature, extract source and calcination temperature of NP synthesis determined the shape and size of the NPs. The incubation time and calcination temperature for the fabrication of silver nanoparticles play a major role in the shape of the nanoparticles. A small variation in the temperature causes a significant change in the structure and shape of AgNPs.

The XRD peaks were also contributed by the phytochemical compounds in the leaf and stem extracts. A similar crystalline nature of silver nanospheres synthesized from Arachis hypogaea using a 1 mM AgNO3 solution was reported.[44] The diffraction peaks obtained in the XRD pattern were at the (111), (200), (220) and (311) planes of a face-centered cubic crystal. Similar results have been reported in recent publications.[45-48]

EDAX predicts the chemical composition and elemental profile of fabricated AgNPs.[49,50] FESEM and EDX analyses provide evident information about the shape, size and elemental composition of the silver nanoparticles. The FESEM images reported the cylindrical shape of AgNPs. Similar forms of cylindrical-shaped AgNPs were reported in earlier experiments.[51] In EDAX analysis, a robust signal of the peak was documented at 3 keV, which is distinctive for the absorption of metallic nanoparticles. The exclusion of other elements authorizes the purity of biogenic nanoparticles. Ag concentrations above 50% in EDAX analysis suggest a notable strength of synthesized AgNPs. Equally, the present study reports the good strength of silver in the biogenic AgNPs, since the element silver was present at a 100% concentration devoid of any trace elements like nitrate.

In UV spectrophotometric analysis, the absorbance peaks were represented by the bioactive constituents in the leaf and stem extracts. The UV absorption spectrum remains in the range of 200 to 300 nm, which is similar to the reports obtained.[52] Photoluminescence analysis exposed the luminescence at 449 nm by the leaf extract and 504 nm by the stem extract could be due to the existence of antioxidants or phytochemical active constituents present in the extracts, respectively. The photoluminescence absorption spectrum revealed an emission peak at 449 nm for both AgNPs and an additional peak at 504 nm for stem-AgNPs was observed. Similar results were documented.[53,54]

Recently, the antibacterial and antifungal activity of this plant species has been acknowledged. The ethanolic leaf extract of *C. rosea* was found to inhibit the bacteriostatic growth of *Staphylococcus epidermidis* at nominal concentrations[55] (Idrus *et al*.,2021). The lectin extracted from the seeds of *Canavalia maritima* (a synonym of *C. rosea*) showed antifungal activity against the fungus *C. neoformans*[56] (Fonseca *et al*., 2022). Some other biological activities of the compounds of *C. rosea* include anti-inflammatory and vasorelaxant effects.[57-60]

Likewise, a recent study validates that ethyl acetate fraction of *Canavalia rosea* leaves prevents ischemia-reperfusion injury. The effect was possible through two synergetic actions, which are the antioxidant effect contributed by flavonoid-like components, quenching free radicals and the increased antioxidant enzyme GPx (Glutathione Peroxidase) activity[61] (Feitosa *et al*., 2023). Moreover, besides preventing oxidative reactions, by their antioxidant capacity, flavonoids are capable of producing anti-inflammatory and anti-platelet aggregation effects, which possibly enhance the rejuvenation of blood in the ischemic zone[62] (Kanaan and Harper 2017).

The antioxidant potential determined by the ABTS assay could be contributed by the bioactive components, such as alkaloids and polyphenols, present in the extract.[63] These results are highly significant when compared to earlier research with mature and young leaves of *C. rosea*, which reported 40% and 45% inhibition, respectively, in the DPPH assay.[64]

The leaf-AgNPs reported the highest percentage of inhibition (87% at 1.95 µg/mL) and the stem-AgNPs exhibited 97% as their highest inhibition percentage at 1.95 µg/mL. These results suggest that both silver nanoparticles possess the potential to be effective cytotoxic sources. In contrast to our results, the cytotoxicity percentage of inhibition at 1 mg/mL of raw and cooked beans of *C. maritima* showed about 31% and 63% in MCF-7 cells.[65]

Another study stated that the leaves of *C. rosea* possess a considerable antioxidant effect, which could contribute to alleviating oxidative stress[59] (Costa *et al.*, 2008). This proves that the biofabricated AgNPs have an enhanced biological response in terms of cytotoxicity. A previous study emphasizes that the pterocarpin derivative, mediacarpin, isolated from Canavalia maritima (a synonym of *Canavalia rosea*), was found to inhibit the growth and proliferation of HeLa cells *in vitro* via apoptotic pathways.[66]

These prior research works emphasize the antibacterial, antifungal and cytotoxic efficiency of *Canavalia* species and hence our vision of AgNP synthesis could be a promising approach in the exploration of anticancer derivatives from *Canavalia rosea*. Also, experiments have proven that silver nanoparticles act as an effective anticancer agent by triggering apoptosis and reactive oxygen species production in cancer cells.[67,68] Although the *in vitro* studies decipher the antioxidant and antiproliferative potential, the effect of silver nanoparticles should be established *in vivo* to authenticate the biological efficacy of the AgNPs.

CONCLUSION

Biogenic synthesis is an exemplary process that elicits a major impact by developing plant-based products. The fabrication of AgNPs from *Canavalia rosea* leaf and stem extracts was documented for the first time. Since earlier studies reported the effective medicinal values of this plant, AgNP production would be a breakthrough. The optical and spectrophotometric analyses acknowledge the shape, structure and stability of the designed AgNPs. The docking interactions of the major phytochemical components of the leaf-AgNPs and stem-AgNPs with the protein targets, estrogen receptor, caspase-9, tumor necrosis factor-α and human epidermal growth factor were deduced. The minimal docking value suggests that these compounds might contribute to the antiproliferative activity against cancer. However, the results should be validated further by *in vitro* and *in vivo* experiments. Nanoparticles confirmed optimistic activity against cancer cells, which could be derived from the assay results. The silver nanoparticles could be further examined for pharmacological uses through the evaluation of mechanisms contributing to their therapeutic potential.

ACKNOWLEDGEMENT

This project was supported by Researchers Supporting Project number (RSP2024R283), King Saud University, Riyadh, Saudi Arabia.

The authors are grateful to the Management, Department of Biotechnology, Physics and Chemistry, of Sri Vinayaga College of Arts and Science, Ulundurpet, Tamilnadu, India for providing laboratory facilities. We are thankful to the Department of Nanoscience, Karunya Institute of Technology and Sciences, Coimbatore and Centralised Instrumentation and Service Laboratory, Department of Physics, Annamalai University, Tamil Nadu, India for providing facilities for characterization analysis. We also extend our thanks to "VIT-SIF Lab, SAS, Chemistry Division for NMR and GC-MS Analysis" for their support in part of this research work.

CONFLICT OF INTEREST

The authors declare that there is no conflict of interest.

ABBREVIATIONS

GC-MS: Gas Chromatography-Mass Spectrometry; **TNF-α:** Tumor-Necrosis Factor-alpha; **HER-2:** Human Epidermal Growth Factor 2; **ER-2:** Estrogen receptor; **CLogP:** Calculated octanol/water partition coefficient; **RCSB PDB:** Research Collaboratory for Structural Bioinformatics Protein Data Bank; **FESEM:** Field Emission Scanning Electron Microscope; **EDAX:** Energy Dispersive X-ray Spectroscopy; **XRD:** X-ray Diffraction; **UV:** Ultraviolet-Visible Spectroscopy; **PL:** Photoluminescence; **µg:** Microgram; **mL:** Millilitre; **MCF-7:** Michigan Cancer Foundation 7; **ROS:** Reactive Oxygen Species; **%:** Percentage; **CSD:** Coastal Sand Dunes (CSD); **ABTS:** 2,2 azino bis (3-ethylbenzothiazoline-6-sulphonic acid) diammonium salt; **min:** Minutes; **°C:** Degree Celsius; **No.1:** Number one; **Leaf-AgNPs:** Leaf extract Silver Nanoparticles; **Stem-AgNPs:** Stem extract Silver Nanoparticles; **Cu-Kα:** Copper-K alpha radiation; **°A:** Angstrom; **JCPDS:** Joint Committee on Powder Diffraction Standards; **ICDD:** International Centre for Diffraction Standards; **nm:** Nanometers; **cm:** Centimetre; **mM:** Milli molar; **A_0:** Absorbance of the control; **A_1:** Absorbance of the sample; **NCCS:** National centre for the Cell Science; **DMEM:** Dulbecco's Modified Eagle medium; **FBS:** Foetal bovine serum; **CO_2:** Carbon dioxide; **MTT:** (3-(4,5-Dimethyl thiazol -2-yl)-2,5-diphenyl tetrazolium bromide); **Cells/mL:** Cells per millilitre; **µL:** Microlitre; **DMSO:** Dimethyl sulfoxide; **IC_{50}:** Half- Maximal Inhibitory Concentration; **PBS:** Phosphate Buffered Saline; **pH:** Potential of Hydrogen; **hr:** Hour; **2θ:** 2 theta (diffraction angle).

SUMMARY

Canavalia rosea is one of the coastal dune families with significant biological potential, such as antioxidant and cytotoxic properties. The green synthesis approach to fabricating AgNPs would be much more important in concluding the importance of this plant species against cancer. *Canavalia rosea* is one of the coastal dune families with significant biological potential, such as antioxidant and cytotoxic properties. The green synthesis approach to fabricating AgNPs would be much more important in concluding the importance of this plant species against cancer.

REFERENCES

1. Zhao Y, Zhang Z, Pan Z, Liu Y. Advanced bioactive nanomaterials for biomedical applications. Exploration. 2021;1:20210089.

2. Sagar Raut D, Thorat RT. Green Synthesis of Zinc Oxide (ZnO) Nanoparticles using *Ocimum tenuiflorum* Leaves. Int J Sci Res. 2015;4:1225-8.
3. Ali A, Zafar H, Zia M, ulHaq I, Phull AR, Ali JS. Synthesis, characterization, applications and challenges of iron oxide nanoparticles. Nanotechnol Sci Appl. 2016;9:49-67.
4. Eid AM, Fouda A, Niedbała G, Hassan SE, Salem SS, Abdo AM, F Hetta H, Shaheen TI. Endophytic Streptomyces laurentii Mediated Green Synthesis of Ag-NPs with Antibacterial and Anticancer Properties for Developing Functional Textile Fabric Properties. Antibiotics (Basel). 2020;9(10):641.
5. Nile SH, Baskar V, Selvaraj D, Nile A, Xiao J, Kai G. Nanotechnologies in Food Science: Applications, Recent Trends and Future Perspectives. Nano Micro Lett. 2020;12:45.
6. Shaheen TI, Salem SS, Zaghloul S. A New Facile Strategy for Multifunctional Textiles Development Through *in situ* Deposition of SiO2/ TiO2 Nanosols Hybrid. Ind Eng Chem Res. 2019;58:20203-12.
7. Mohmed AA, Fouda A, Elgamal MS, El-Din Hassan S, Shaheen TI, Salem SS. Enhancing of cotton fabric antibacterial properties by silver nanoparticles synthesized by new Egyptian strain *Fusarium keratoplasticum* A1-3. Egypt J Chem. 2017;60:63-71.
8. Kathiravan V, Ravi S, Ashok Kumar S. Synthesis of Silver Nanoparticles from *Melia dubia* Leaf Extract and Their *in vitro* Anticancer Activity. Spectrochim Acta A: Mol Biomol Spectrosc. 2014;130:116-21.
9. Castellano JJ, Shafii SM, Ko F, Donate G, Wright TE, Mannari RJ, Payne WG, Smith DJ, Robson MC. Comparative evaluation of silver-containing antimicrobial dressings and drugs. Int Wound J. 2007;4:114-22.
10. Alsammarraie FK, Wang W, Zhou P, Mustapha A, Lin M. Green synthesis of silver nanoparticles using turmeric extracts and investigation of their antibacterial activities. Colloids Surf B: Biointerface. 2018;171:398-405.
11. Heinlaan M, Ivask A, Blinova I, Dubourguier HC, Kahru A. Toxicity of Nanosized and Bulk ZnO, CuO and TiO_2 to Bacteria *Vibrio fischeri* and Crustaceans *Daphnia magna* and *Thamnocephalus platyurus*. Chemosphere. 2008;71:1308-16.
12. Qu J, Yuan X, Wang X, Shao P. Zinc Accumulation and Synthesis of ZnO Nanoparticles Using *Physalis alkekengi* L. Environ Pollut. 2011;159:1783-8.
13. Vasanthi R, Balamurugan V. Preliminary Phytochemical Screening of Leaf and Stem Extracts of *Canavalia rosea*. Res J Agri Sci. 2023;14(1):99-104.
14. Arun AB, Beena KR, Raviraja NS, Sridhar KR. Coastal sand dunes - A neglected ecosystem. Curr Sci. 1999;77:19-21.
15. Bhagya B, Sridhar KR, Raviraja NS, Young CC, Arun AB. Nutritional and biological qualities of ripened beans of *Canavalia maritima* of coastal sand dunes of India. Compt Rend Biol. 2009;332:25-33.
16. Morris JB. Legume genetic resources with novel value-added industrial and pharmaceutical use, In: Perspectives on New Crops and New Uses, edited by J Janick, 1999;196-201, ASHS Press, Alexandria, VA, USA.
17. Huang X. Pterocarpin and Isoflavan Derivatives from *Canavalia maritime* (Aubl.) Thou Rec Nat Prod. 2012;6(2):166-70.
18. Venugopal K, Rather HA, Rajagopal K, Shanthi MP, Sheriff K, Illiyas M, *et al.* Synthesis of silver nanoparticles (Ag NPs) for anticancer activities (MCF 7 breast and A549 lung cell lines) of the crude extract of *Syzygium aromaticum*. J Photochem Photobio B: Bio. 2017;167:282-9.
19. Benet LZ, Hosey CM, Ursu O, Oprea TI. BDDCS, the Rule of 5 and drug ability. Adv Drug Deliv Rev. 2016;101:89-98.
20. Kim S. Exploring chemical information in PubChem. Current Protocols. 2021;1(8):e217.
21. O'Boyle NM, Banck M, James CA, Morley C, Vandermeersch T, Hutchison GR, Open Babel. An open chemical toolbox. J Cheminf. 2011;3(1):1-4.
22. Morris GM, Huey R, Lindstrom W, Sanner MF, Belew RK, Goodsell DS, *et al*. AutoDock4 and AutoDockTools4: automated docking with selective receptor flexibility. J Comput Chem. 2009;30(16):2785-91.
23. Shiozaki EN, Chai J, Rigotti DJ, *et al.* Mechanism of xiap-mediated inhibition of caspase-9. Molecular Cell. 2003;11(2):519-27.
24. Tanenbaum DM, Wang Y, Williams SP, Sigler PB. Crystallographic comparison of the estrogen and progesterone receptor's ligand binding domains. Proc Natl Acad Sci USA. 1998;95(11):5998-6003.
25. Eck MJ, Sprang SR. The structure of tumor necrosis factor-alpha at 2.6 A resolution. Implications for receptor binding. J Biol Chem. 1989;264:17595-605.
26. Aertgeerts K, Skene R, Yano J, *et al.* Structural analysis of the mechanism of inhibition and allosteric activation of the kinase domain of her2 protein. J Biol Chem. 2011;286(21):18756-65.
27. Re R, Pellegrini N, Proteggente A, Pannala A, Yang M, Rice-Evans C, Antioxidant activity applying an improved ABTS radical cation decolorizing assay. Free Radical Bio Medi.1999;26: 1231-7.
28. Mosmann T. Rapid colorimetric assay for cellular growth and survival: application to proliferation and cytotoxicity assay. J Immunol Methods. 1983;65:55-63.
29. Chibuzo OU, Okop I. Chemical Information from GCMS analysis of acetone extract of *Piper guineense* leaves. J Phys Communication. 2020;5:437-445.
30. NIST Chemistry WebBook, Mallard, W.G., Linstrom, P.J., Eds. NIST Standard Reference Database, National Institute of Standards and Technology, (2008) (https://webbook .nist.gov).
31. Prabhu S, Joelri Michael Raj L, John Britto S, Senthilkumar S. Antibacterial activity and preliminary phytochemical analysis of leaf extract of *Canavalia rosea* (Sw.) DC. (Beach Bean). Int J Res Pharm Sci. 2010;1:428-34.
32. Aswathi V, Abdussalam AK. Determination of energy content, phytochemical constituents and antioxidant activity of potential wild edible legume; *Canavalia rosea* (sw.) dc. from Northern Kerala. Int J Curr Pharm Res, 2020;12(5):86-9.
33. Madziga HA, Sanni S, Sandabe UK. Phytochemical and elemental analysis of *Acalypha wilkesiana* leaf. J Am Sci. 2010;6(11):510-4.
34. Sarker SD, Nahar L. Chemistry for Pharmacy Students General, Organic and Natural Product Chemistry. England: John Wiley and Sons. 2007:283-359.
35. Kar A. Pharmacognosy and Pharmacobiotechnology (Revised-Expanded Second Edition). New Age International Limited Publishers New Delhi. 2007:332-600.
36. Chibuzo OU, Okop I. Chemical Information from GCMS analysis of acetone extract of *Piper guineense* leaves. J Phys Communication. 2020;5:437-45.
37. Jay TM, Dienel GA, Cruz NF, Mori K, Nelson T, Sokoloff L. Metabolic stability of 3-O-methyl-d-glucose in brain and other tissues. J Neurochem. 1990;55:989-1000.
38. Sehgal AA, Li Y, Lal B, Yadav NN, Xu X, Xu J, Laterra J, van Zijl PCM. CEST MRI of 3-O-methyl-glucose uptake and accumulation in brain tumors. Magnetic Resonance Med. 2018;81:1993-2000.
39. Vijayalakshmi K, Priya V, Jananie K. https://www.jocpr.com/articles/gcms-determination-of-bioactive-components-oftrigonella-foenum-grecum.pdf. J Chem Pharm Res. 2011;5:35-40.
40. Liu J, Lee GY, Lawitts JA, Toner M, Biggers JD. Preservation of Mouse Sperm by Convective Drying and Storing in 3-O-Methyl-D-Glucose. PLoS ONE. 2012;7(1):e29924.
41. Yugandhar P, Kumar KK, Neeraja P, Savithramma N. Isolation, characterization and *in silico* docking studies of synergistic estrogen receptor a anticancer polyphenols from *Syzygium alternifolium* (Wt.) Walp. J Intercult Ethnopharmacol. 2017;6:296-310.
42. Prabhakar M, Manoharan S, Ignacimuthu S, Stalin A. *In silico* docking analysis to explore the proapoptotic and anti-cell proliferative potential of ferulic acid. Indian J Biochem Biophys. 2016;53:17-23.
43. Nivetha R, Meenakumari M, Bhuvaragavan S, Hilda K, Janarthanan S. *In silico* analysis of carbohydrate-binding pockets in the lectin genes from various species of Canavalia. Comp Biol Chem. 2021;92:107477.
44. Varadavenkatesan T, Pai S, Vinayagam R, Selvaraj R. Characterization of silver nano-spheres synthesized using the extract of *Arachis hypogaea* nuts and their catalytic potential to degrade dyes. Mat Chem Phys. 2021;272:125017.
45. Jyoti K, Baunthiyal M, Singh A. Characterization of silver nanoparticles synthesized using *Urtica dioica* Linn. leaves and their synergistic effects with antibiotics. J Radiat Res Appl Sci. 2016;9:217-27.
46. Ghotekar S, Savale A, Pansambal S. Phytofabrication of fluorescent silver nanoparticles from *Leucaena leucocephala* L. leaves and their biological activities. J Water Environ Nanotechnol. 2018;3(2):95-105.
47. Ghotekar S, Pansambal S, Pawar SP, Pagar T, Oza R, Bangale S. Biological activities of biogenically synthesized fluorescent silver nanoparticles using *Acanthospermum hispidum* leaves extract. SN App Sci. 2019;1:1342.
48. Hashem AH, El-Sayyad GS, Al-Askar AA, Marey SA, AbdElgawad H, Abd-Elsalam KA, Saied E. Watermelon Rind Mediated Biosynthesis of Bimetallic Selenium-Silver Nanoparticles: Characterization, Antimicrobial and Anticancer Activities. Plants. 2023;12:3288.
49. Sumra AA, Aadil M, Ejaz SR, Anjum S, Saleem T, Zain M, Alsafari IA. Biological synthesis of nanostructured ZnO as a solar-light driven photocatalyst and antimicrobial agent. Ceram Int. 2022;48:14652-61.
50. Alula MT, Lemmens P, Bo L, Wulferding D, Yang J, Spende H. Preparation of silver nanoparticles coated ZnO/Fe3O4 composites using chemical reduction method for sensitive detection of uric acid via surface-enhanced Raman spectroscopy. Anal Chim Acta. 2019;1073:62-71.
51. Pal S, Tak YK, Song JM. Does the antibacterial activity of silver nanoparticles depend on the shape of the nanoparticle? A study of the Gram-negative bacterium *Escherichia coli*. Appl Environ Microbiol. 2007;73(6):1712-20.
52. Mercado-Meza DY, Guevara-Gonzalez RG, Esquivel K, Carbajal-Valenzuela I, Avila-Quezada GD. Green silver nanoparticles display protection against *Clavibacter michiganensis* subsp. michiganensis in tomato plants (*Solanum lycopersicum* L.). Plant Stress. 2023;10:100256.
53. Anandalakshmi K, Venugobal J, Ramasamy V. Characterization of silver nanoparticles by green synthesis method using *Pedalium murex* leaf extract and their antibacterial activity. Appl Nanosci. 2016;6:399-408.
54. Khan SH, Patel S, Shukla P, Kumar R, Dixit R. Synthesis of silver nanoparticles by green method using *Ligustrum sinense* to study their structural and photoluminescence properties. Eurasian J Phys Func Mat. 2023;7(1):52-9.
55. Idrus I, Kurniawan F, Mustapa F and Wibowo D. Concentration effect of leaf extract from Kekara Laut (*Canavalia maritima* Thou.) in inhibiting of *Staphylococcus epidermidis* bacteria with a statistical science approach. Indo J Chem Res. 2021;8(3):180-5.
56. Fonseca VJA, Braga AL, de Almeida RS, da Silva TG, da Silva JCP and de Lima LF. Lectins ConA and ConM extracted from *Canavalia ensiformis* (L.) DC and *Canavalia rosea* (Sw.) DC inhibit planktonic *Candida albicans* and *Candida tropicalis*. Arch Microbiol. 2022;204(6):346.
57. Assreuy AMS, Fontenele SR, De Freitas Pires A, *et al.* Vasodilator effects of *Diocleinae lectins* from the *Canavalia* genus. Naunyn-Schmied Arch Pharmacol. 2009;380(6):509-21.
58. Bezerra GA, Oliveira TM, Moreno FBMB, *et al.* Structural analysis of *Canavalia maritima* and *Canavalia gladiata* lectins complexed with different dimannosides: New insights

into the understanding of the structure-biological activity relationship in legume lectins. Journal of Structural Biology. 2007;160(2):168-76.

59. Costa CRA, Figueroa MA andrade YB and Barreiros AL BS. 2008. Atividade antioxidante dos extratos de folhas e caule de *Canavalia*. S B. Q: 1.
60. Pattamadilok D, Pengsuparp T, Phummiratch D, *et al.* Canarosine: A new guanidine alkaloid from *Canavalia rosea* with inhibitory activity on dopamine D1 receptors. Journal of Asian Natural Products Research. 2008;10(10):915-8.
61. Feitosa MBJ, Araújo SS, Mesquita TRR, *et al.* Antioxidants and cardioprotective effects of ethyl acetate fraction of *Canavalia rosea* leaves in myocardial ischemia-reperfusion injury. An Acad Bras Ciênc. 2023;95(suppl 1):e20220514.
62. Kanaan GN, Harper ME. Cellular redox dysfunction in the development of cardiovascular diseases. Biochim Biophys Acta Gen Subj. 2017; 1861(11 Pt A):2822-9.
63. Docea AO, Calina D, Buga AM. The Effect of silver nanoparticles on antioxidant/ Pro-oxidant balance in a murine model. Int J Mol Sci. 2020;21(4):1233.
64. Nivas D, Sonar BA, Shaikh SS, Patil UH, Gaikwad DK, Chavan NS, Sabale AB, Chavan PD. Screening of some coastal plant resources for their antioxidant potential, total polyphenol and flavonoid content. Pharmacogn Mag. 2010;2(7):151-6.
65. Niveditha VR, Divana V, Sridhar K. Cytotoxic effects of methanol extract of raw, cooked and fermented split beans of *Canavalia* on cancer cell lines MCF-7 and HT-29. Institute Integ Omic App Biotech J. 2013;4:20-3.
66. Xu MJ, Huang XP, Li M, Sun W, Cui JR, Lin WH. Cytotoxic and pro-apoptotic activities of medicarpin from *Canavalia maritima* (Aubl.) via the suppression of NF-KB activation in HeLa cells. J Chinese Pharmaceu Sci. 2009;18:331-6.
67. Gurunathan S, Han J, Eppakayala W, Jeyaraj VM, Kim JH. Cytotoxicity of biologically synthesized silver nanoparticles in MDA-MB-231 human breast cancer cells. Biomed Res Int. 2013;535796.
68. Al-Brahim JS, Mohammed AE. Antioxidant, cytotoxic and antibacterial potentials of biosynthesized silver nanoparticles using bee's honey from two different floral sources in Saudi Arabia. Saudi J Biol Sci. 2020;27:363-73.

Cite this article: Vasanthi R, Balamurugan V, Almoallim HS, Alharbi SA. Biosynthesis of Silver Nanoparticles from *Canavalia rosea* and its Antiproliferative Effect on MCF-7 Cancer Cell Line. Indian J of Pharmaceutical Education and Research. 2024;58(3s):s944-s962.